RESEARCH ARTICLE

Formation of present desert landscape surrounding Jilantai Salt Lake in northern China based on OSL dating

Yuxin FAN (✉)[1,2], Xiaolong CHEN[1], Wenhao LIU[1], Fu ZHANG[1], Fan ZHANG[1]

1 School of Earth Sciences and Key Laboratory of Mineral Resources in Western China of Gansu Province, Lanzhou University, Lanzhou 730000, China
2 MOE Key Laboratory of Western China's Environmental Systems, Collaborative Innovation Center for Arid Environments and Climate Change, Lanzhou University, Lanzhou 730000, China

Abstract The Jilantai Salt Lake (JSL), a lake of importance due to its salt production in China since the early Qing dynasty, is surrounded by sand dunes. Exploration of the development of these sand dunes will be helpful for identifying the forces underlying the desert landscape and for identifying a solution to protect the salt resources. Through field investigation, we found sand dunes overlying either lacustrine and bog deposits on the lake bed at a lower altitude or littoral sediments on the higher lakeshores. Optically Stimulated Luminescence (OSL) dating results indicate that sands started to accumulate around the JSL as early as the early Holocene (around 11 ka), while the rapid development of sand dunes occurred within the latest 0.1 ka. By comparison with climatic documents and human activities in adjacent regions, the initiation of sand accumulation around the JSL as early as the early Holocene is considered to be the result of low effective moisture in the Jilantai area. However, the rapid development of the sand dunes in the vast area surrounding the JSL was likely initiated by the intensified human activities which occurred within the latest 0.1 ka under warm and dry climatic conditions.

Keywords aeolian sand accumulation, Jilantai Salt Lake, OSL dating

1 Introduction

The Jilantai Salt Lake (JSL), surrounded on the southeast by the Ulan Buh Desert, is situated on the eastern Alashan Plateau, the western margin of the present East Asian

summer monsoon domain (An et al., 2005). This region is also a transitional belt between arid and semiarid China (Wang, 1989). JSL has been an important source of salt production, supplying salt to adjacent provinces, such as Shaanxi, Gansu, and Shanxi, since the Qing Dynasty or even earlier (Wang and Dou, 1998). However, current production associated with the JSL is being seriously affected by sand desert invasion (Geng and Hu, 1989; Wang, 1989; Geng and Chen, 1990). Some previous work in this area indicates that sand dune invasion in the JSL is the result of large scale human activity over the past 50 years (Geng and Hu, 1989, 1990; Wang, 1989). Alternatively other studies assert that these sand dunes were formed since around 7 ka as a result of the shrinkage of the Jilantai megalakes and sand blown from the exposed loose sediments (Chun et al., 2008). Therefore, it is still unclear when and why the present desert landscape surrounding the JSL formed. In this paper, we investigate the sedimentary sequence beneath the sand dunes with the utilization of remote sensing images. We obtained the initiation ages of some sand dunes around the JSL by using the Optically Stimulated Luminescence (OSL) dating technique with the aim of identifying when and how this desert landscape formed.

2 Study area

The JSL (39°37′–39°40′N, 105°29′–105°41′E) is centrally located in the catchment between the Bayan Ulan Mountains and the Helan Mountains (Fig. 1), i.e., the Jilantai Basin on the eastern Alashan Plateau. The present Ulan Buh Desert lies to the east of the JSL (Geng and Chen, 1990). The JSL, one of China's most important sources of salt production, covers an area of $102.4 \, \text{km}^2$, and lies at an altitude of approximately 1,022.6 m. Three
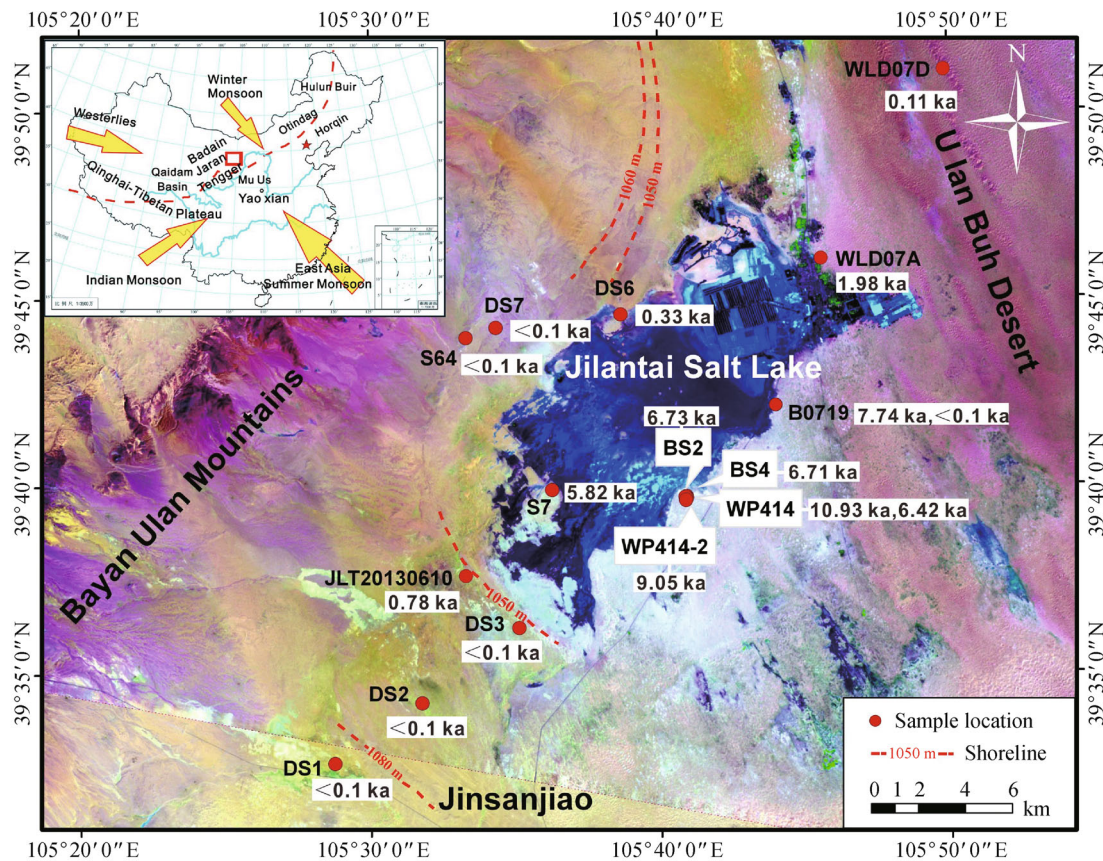
Fig. 1 Study area and sample sites around the JSL. Profiles WLD07D and WLD07A are from Fan et al. (2010); BS2, BS4, and S7 are from Fan (2008).

cyclic sand belts surrounding the JSL on its southwest banks were identified from remote sensing images (Wang, 2001). Through field investigations, it was determined that these sand belts formed by sand accumulation on its lakeshores (Chen et al., 2008; Yang et al., 2008). In addition, the desert landscape was found to be primarily composed of crescent, longitudinal, and coronary dunes.

The prevailing wind in the JSL basin is from the southwest, with an annual wind speed ranging from 3.3 m/s to 21 m/s (Pang and Hu, 2009). The annual precipitation and evaporation are 113.56 mm and 3,023.7 mm, respectively.

3   Sedimentary sequence and OSL samples

We investigated the sedimentary sequence through 12 profiles arranged in two radial sections from the salt lake to the higher shores on the southwest bank of the lake. Analysis of the sedimentary sequence of the sand dunes or sand hills (Table 1) supports the idea that the present desert landscape was developed above either the lake bed composed of lacustrine and bog deposits found at lower altitudes or littoral sediments found on the higher

lakeshores.

The sedimentary sequence of profiles situated on the high southern and western shores, at altitudes between 1,080 and 1,050 m a.s.l., e.g., DS1, DS2, DS3, JLT20130610, DS7, and S64, supports the assertion that aeolian sand accumulated above the lakeshores which were primarily composed of littoral sediments formed during the Jilantai-Hetao Megalake and Jilantai-Hetao Main Lake phases (Fan, 2008). Aeolian sand found at lower altitudes accumulated above either the shores formed during the Jilantai paleolake phase or lacustrine and bog deposits which formed later. For example, in profiles BS4, DS6, and WP414, aeolian sand overlay the layers mainly composed of sandy clay or clayey silt. In summary, sand dunes surrounding the JSL accumulated above either lacustrine and bog deposits or paleo-lakeshores formed at different stages.

To obtain the initiation time of sand accumulation, we collected samples from the bottom layer of the sand dunes and hills (Figs. 2 and 3) for OSL dating. Stainless steel sampling tubes were hammered horizontally into the bottom layer of each sand dune to collect the samples. Both ends of these tubes were then quickly sealed with light-proof tape once they were removed.

Table 1 Sedimentary sequence observed from the exposure through the base of sand dunes/hills surrounding the JSL. Description of profiles BS2 and BS4 is from Chun et al. (2008)

Profile	Coordinate and altitude (m a.s.l.)	Geomorphic type	Sedimentary sequence
DS1	N 39°32′36.3″ E 105°28′46.2″ 1,080 m	Dune on the 1,080 m lakeshore southwest of the JSL	0–50 cm: Light brownish aeolian sand. OSL sample DS1–40 was collected at 40 cm depth; 50–60 cm: Grayish white clayey sand; 60–100 cm: Brownish red silty fine sand; 100–170 cm: Littoral sandy gravels, thicker than 70 cm
DS2	N 39°34′12.9″ E 105°31′45.6″ 1,065 m	Dune on the 1,060 m lakeshore southwest of the JSL	0–130 cm: Light yellowish aeolian sand. OSL sample DS2-120 was collected at 120 cm depth; 130–150 cm: Littoral sandy gravels, thicker than 70 cm
DS3	N 39°36′12.5″ E 105°35′07.5″ 1,052 m	Dune on the 1,050 m lakeshore southwest of the JSL	0–120 cm: Light yellowish aeolian sand. OSL sample DS3-110 was collected at 110 cm depth; 120–140 cm: Brownish red silty clay, thicker than 20 cm
WP414	N 39°39′41.9″ E 105°40′55.4″ 1,020 m	Excavated pit on a sandy beach southeast of the JSL with altitude of 1,020 m	0–3 cm: White calcium carbonate layer; 3–37 cm: Light yellowish fine sand; 37–42 cm: Brownish red fine sand, with calcium carbonate consolidated; 42–150 cm: Light yellowish fine sand. OSL sample WP414-100 was collected at 100 cm depth; 150–200 cm: Grayish lacustrine clayey silt, thicker than 50 cm
WP414-2	N 39°39′310.9″ E 105°40′55.8″ 1,021 m	Dune on a sandy beach southeast of the JSL with altitude of 1,021 m	0–150 cm: Light yellowish aeolian sand. OSL sample WP414-2-140 was collected at 140 cm depth; 150–180 cm: Grayish coarse sand below the level of the interdune depression
BS2	N 39°39′41″ E 105°40′53″ 1,030 m	Excavated pit on a sandy beach southeast of the JSL with altitude of 1,030 m	0–10 cm: Brownish red sandy clay; 10–80 cm: Grayish yellow aeolian sand, thicker than 50 cm. OSL sample OSL-4 was collected at 40 cm depth
BS4	N 39°39′36″ E 105°40′54″ 1,032 m	Excavated pit on a sandy beach southeast of the JSL with altitude of 1,032 m	0–10 cm: Brownish red sandy clay; 10–80 cm: Light yellowish fine sand. OSL sample OSL-10 was collected at 70 cm depth; 80–100 cm: Grayish lacustrine sandy clay, thicker than 140 cm
JLT20130610	N 39°37′54″ E 105°33′40″ 1,050 m	Outcrop (sand quarry) on the 1,050 m lakeshore	0–10 cm: Fine sand with fine rounded and well sorted pebbles; 10–160 cm: Light yellowish aeolian sand, plant residue and black root-canals preserved. OSL samples JLT20130610-80 and JLT20130610-140 were collected at 80 cm and 140 cm depth respectively; 160–200 cm: Grayish fine silt sand with very fine pebbles (diameter of 2–3 mm); 200–220 cm: Pebbly sandstone, poorly sorted and rounded, thicker than 20 cm
DS6	N 39°44′33.5″ E 105°38′41″ 1,032 m	Dune on the 1,032 m lakeshore west of the JSL	0–100 cm: Light yellowish aeolian sand. OSL sample DS6-90 were collected at 90 cm depth; 100–113 cm: Blackish silty clay; 113–150 cm: Light yellowish fine sand, thicker than 37 cm, OSL sample DS6-125 were collected at 125 cm depth
DS7	N 39°44′11.3″ E 105°34′21.9″ 1,048 m	Dune on the 1,050 m lakeshore west of the JSL	0–100 cm: Light yellowish aeolian sand. OSL sample DS7-90 was collected at 90 cm depth; 100–125 cm: Littoral sandy gravels. OSL sample DS7-110 was collected at 110 cm depth; 125–130 cm: Brownish red clayey silt, thicker than 37 cm
S64	N 39°43′56.9″ E 105°33′19.5″ 1,060 m	Dune on the 1,060 m lakeshore west of the JSL	0–80 cm: Light yellowish aeolian sand. OSL samples S64-65 and S64-75 were collected at 65 cm and 75 cm depth respectively; 80–90 cm: Littoral sandy gravels; 90–120 cm: Grayish yellow Lacustrine clay, thicker than 30 cm

| Profile	Coordinate and altitude (m a.s.l.)	Geomorphic type	Sedimentary sequence
B0719	N 39°42′07″ E 105°44′03″ 1,026 m	Excavated pit on the 1,026 m beach southeast of the JSL	0−60 cm: Light yellowish aeolian sand. OSL sample B0719-60 was collected at 60 cm depth; 60−80 cm: Brownish red desert soil; 80−90 cm: Grayish fine sand; 90−95 cm: Grayish-green clay; 95−120 cm: Grayish green fine sand, mollusk shells preserved; 120−150 cm: Grayish green silty clay; 150−230 cm: Grayish fine sand, mollusk shells preserved; 230−280 cm: Grayish calcium carbonate consolidated fine sand, thicker than 50 cm. Groundwater appeared at 280 cm depth. OSL sample B0719-240 was collected at 240 cm depth
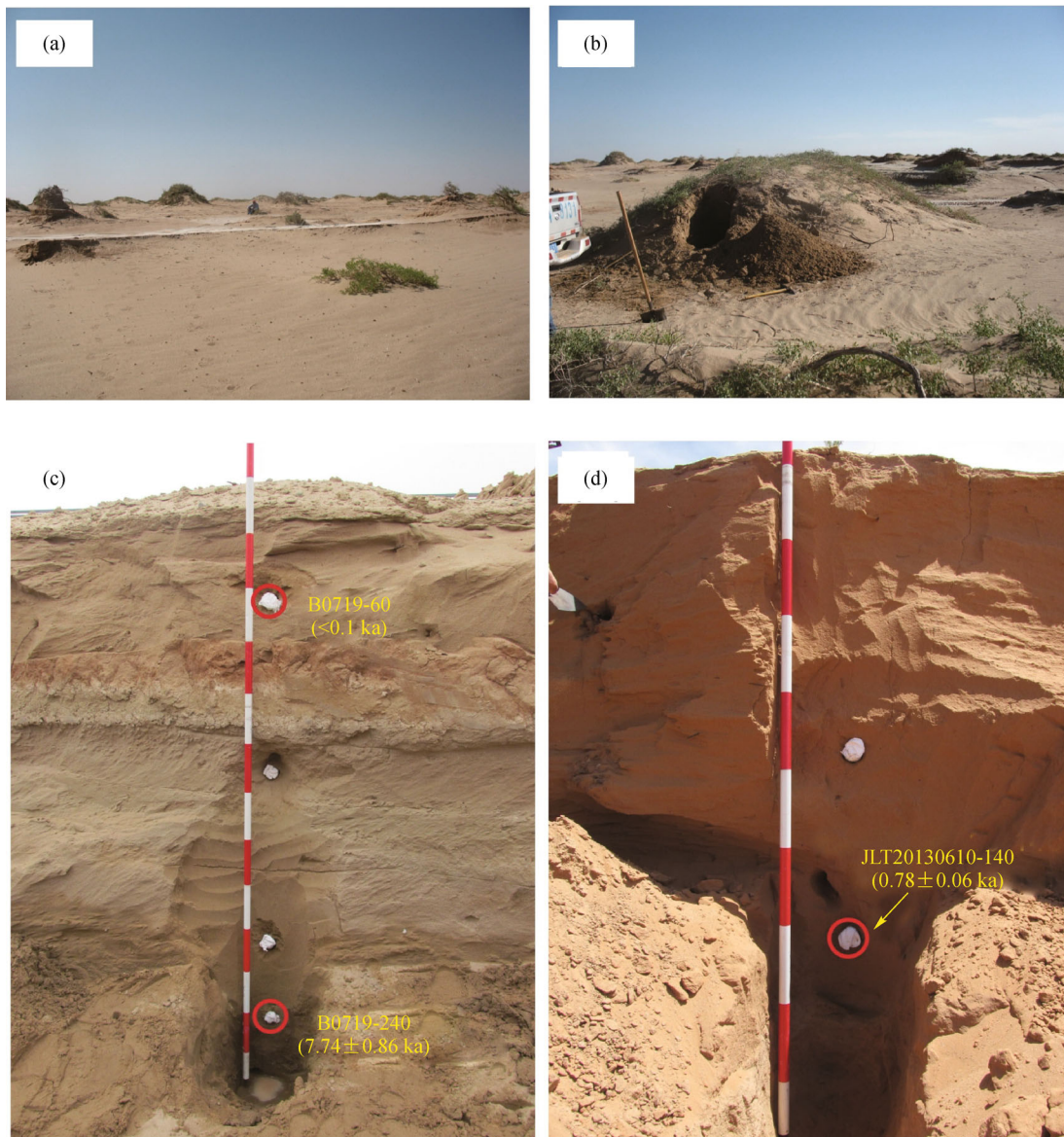
Fig. 2 Photos of the representative profiles and landscape surrounding the JSL: (a) landscape southeast of the JSL; (b) Profile WP414-2; sedimentary sequence of profiles (c) JLT20130610 and (d) B0719.
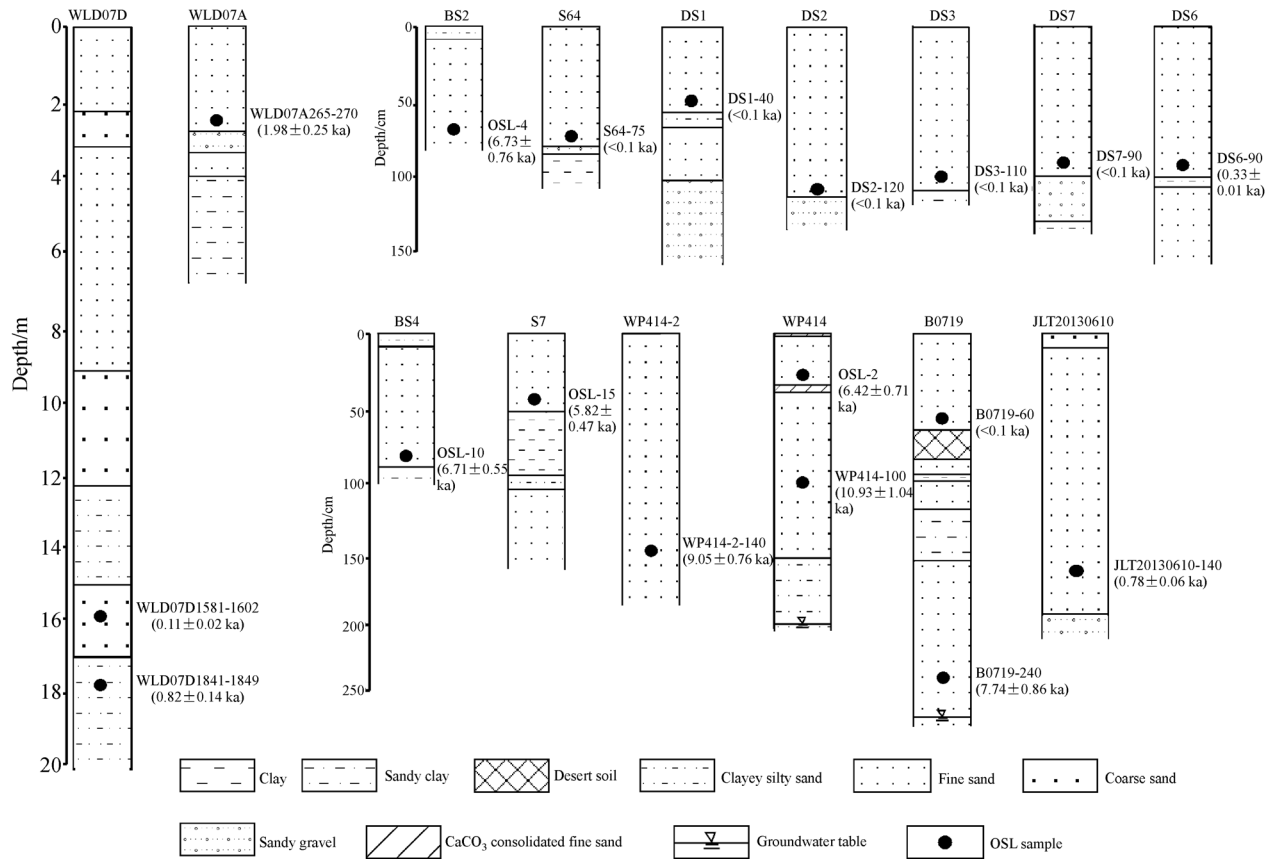
Fig. 3 Sedimentary sequence and OSL dating results. The data of profiles BS2 and BS4 are from Chun et al. (2008). S7 is a sand dune situated on a spring mound, and data of this section are from Fan (2008). Data of sand dunes / hills WLD07D and WLD07A are from Fan et al. (2010).

4 Method and results

4.1 Dating methods

The OSL dating method is applied to measure the initiation ages of sand accumulation in this study. OSL signals were measured from quartz fractions. The extraction of quartz fractions and OSL signal measurements were performed in the MOE Key Laboratory of Western China's Environmental Systems at Lanzhou University. The 90−125 μm quartz fractions were extracted in a dark room with subdued red light using a traditional separation method (Fan et al., 2010). The purity of the quartz fractions was checked by the absence of infrared stimulated luminescence signal (IRSL) under 50°C. To eliminate the potential contribution of any IRSL signal from the feldspar inclusions hosted in the quartz crystals, the modified post-IR OSL protocol (Banerjee et al., 2001), as listed in Table 2, was employed to measure the OSL signal from the quartz fractions. However, large errors may be induced to the ratio of Li/Ti, and consequently the equivalent dose (D_e) value, when a small test dose is used, even though D_e is very insensitive to the size of the test dose (Murray and Wintle, 2000). Therefore, a test dose of 4.4 Gy was applied

Table 2 The protocol used in this paper

Step	Operation	Observation
1	Given dose, $D_i(i = 0,1,2…, D_0= 0)$	
2	Preheat at (160−260)°C for 10 s	
3	Infrared stimulation for 40 s at 50°C	
4	Blue stimulation for 40 s at 125°C	Li
5	Given test dose, D_T	
6	Cutheat at 160°C	
7	Infrared stimulation for 40 s at 50°C	
8	Blue stimulation for 40 s at 125°C	Ti
9	Illumination at 280°C for 40 s	
10	Return to step 1	

to the measurement in this study.

Recent studies show that D_e values are highly sensitive to the preheat temperature of some samples (Wintle and Murray, 2006; Roberts, 2012). Therefore, to select the most appropriate preheat temperature for the D_e measurement, we performed a dose recovery test for each sample by increasing the preheat temperature from 160°C to 260°C at 20°C intervals. The procedures used for detailed

measurement are the same as those utilized in Fan et al. (2013). Only the preheat temperature, with both the dose recovery and recycling ratios within 10% of unity and recuperations less than 5%, was employed to the protocol to measure the OSL signal and D_e values of the sample.

The environmental dose rate was calculated from the radioactive element contents of Uranium (U), Thorium (Th), and Potassium (K) in the sample, and its closely surrounding sediments, with a contribution from cosmic rays. In this study, the concentration of U and Th, and the content of K were determined by means of Neutron Activation Analysis (NAA). The concentration of these elements was converted into beta and gamma dose rates according to the conversion factors given in Aitken (1985). The dose rate from cosmic rays was calculated according to the burial depth, latitude and altitude where the samples were collected (Prescott and Hutton, 1994). Due to uncertainties of water content in the sediments during the burial periods, the average water content was estimated according to both the natural and saturated water content measured in the laboratory. Finally, the total dose rate was calibrated by using the estimated water content as listed in Table 3.

4.2 OSL dating results

OSL signals of 11 samples were measured in this study. For samples B0719-60, DS1-40, DS2-120, DS3-110, DS7-90, and S64-75, there was no obvious decay of the natural OSL signals; whereas, obvious decay was observed in their signals to the laboratory-given dose for either the regenerated dose (e.g., 2.2 Gy) or the test dose (4.4 Gy) (Fig. 4(a)). The absence of decay in natural OSL signals is

deduced to be the result of very recent accumulation (< 0.1 ka), which is also supported by the very small equivalent dose (< 0.3 Gy) of the brightest aliquots, as illustrated in the inset in Fig. 4(a). Other samples, e.g., WP414-100 and DS1-40, show a normal decay (Fig. 4(b)) with equivalent doses between 2 Gy and 26 Gy (Table 3). The D_e values of 2–26 Gy distributed within the linear growth segment (see the inset of Fig. 4(b)), supporting the basis for no age underestimation due to dose saturation.

The D_e values distribution of different aliquots of the samples are illustrated as histograms in Fig. 5. The D_e values of most samples are concentrated with small relative standard deviation (RSD < 0.32) (e.g., Figs. 5(a)–(d), (g), and (i)), supporting that these samples were well-bleached before burial; therefore, D_e values of all qualified aliquots were used to calculate the D_e value of these samples. However, D_e values of aliquots for samples OSL-2 and OSL-10 were scattered (Figs. 5(e) and 5(f)) with RSD values greater than 0.32 (RSD = 0.41 and 0.42) for all qualified aliquots, indicating that these two samples were poorly bleached. After rejection of the outliers with large D_e values, which were obviously deviated, the distribution of D_e values became concentrated with a small RSD value (< 0.3). Finally, the D_e values of these two samples were calculated based on those concentrated D_e values represented by the shadowed columns in the histograms in Figs. 5(e) and 5(f).

The OSL ages were calculated by dividing the D_e values by the dose rates, as shown in Table 3 and illustrated in Figs. 2 and 3. These dating results support the idea that the initiation time of the present desert landscape around JSL is clustered into three intervals: 10.9–9.0 ka, 6.7–5.8 ka, and within the latest 2 ka, especially within the latest 0.1
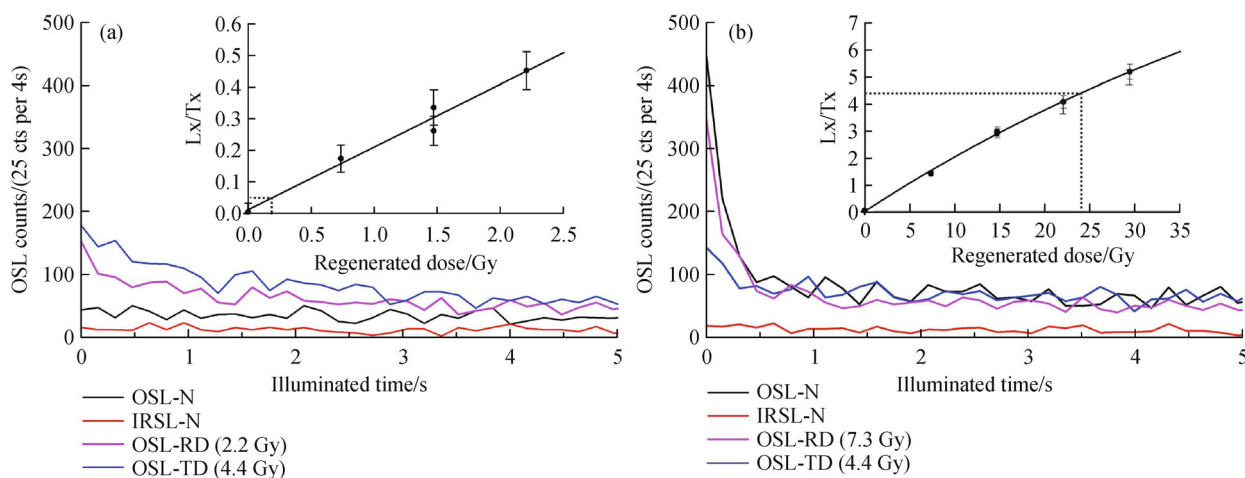

Fig. 4 Decay curves within the original 5 s of natural OSL and IRSL signals, as well as a laboratory-given regenerated dose and the test dose for the representative samples: (a) DS1-40 and (b) WP414-100. The inset of (a) is the growth curve of the brightest aliquot in the sample DS1-40, and the inset of (b) is the growth curve of the representative aliquot in the sample WP414-100. OSL-N and IRSL-N represent the decay curve of the natural OSL signal and the natural IRSL signal for one aliquot, respectively. OSL-RD and OSL-TD represent the decay curve of OSL signals for a regenerated dose and the test dose given in the laboratory, respectively.
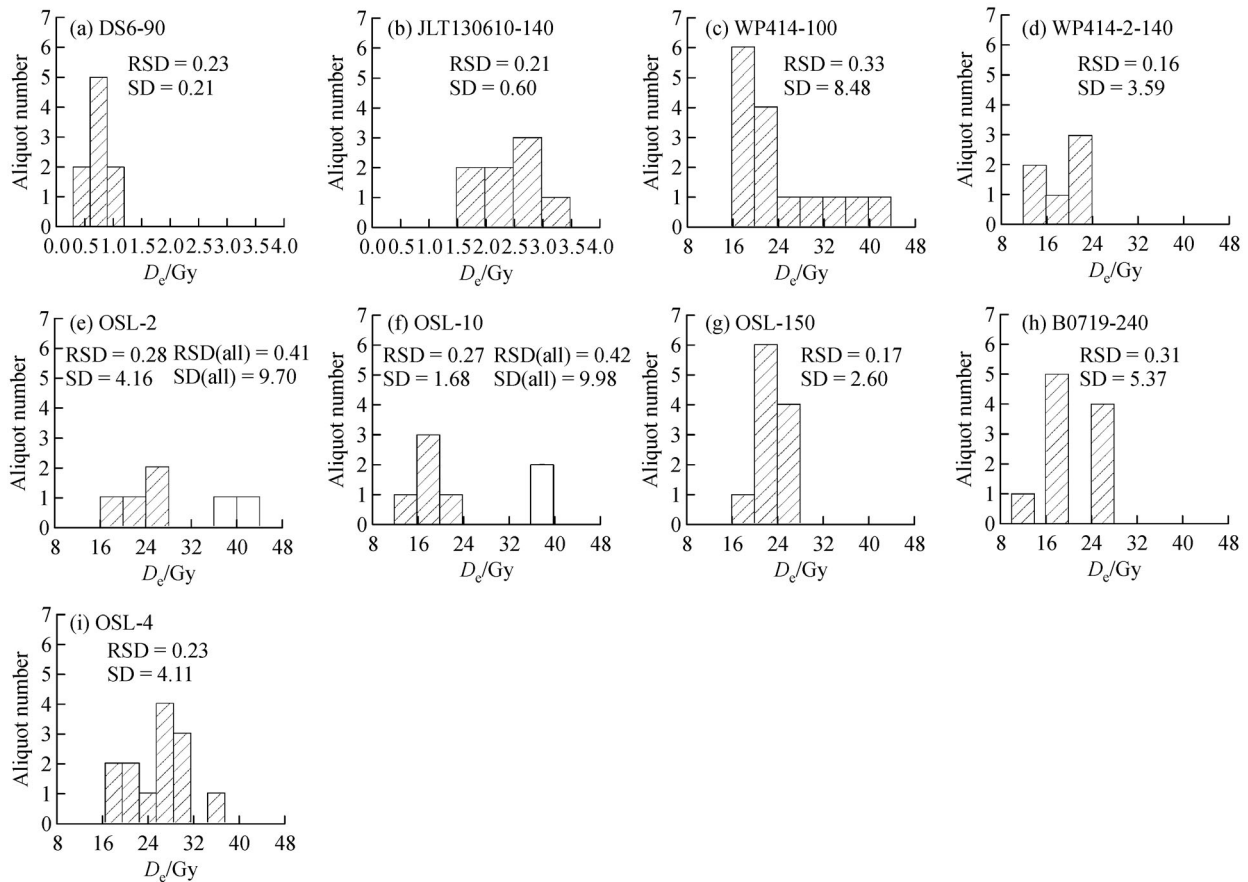
Fig. 5 Histograms of D_e values of different aliquots for the samples studied. The shadowed histograms represent the aliquots which were used for calculation of the D_e value of the sample, and the unfilled histograms represent outliers.

ka, respectively (Fig. 5).

For the purpose of visually demonstrating the initiation time of the present desert landscape around the JSL, we assume that there was a 0 depth line at the bottom of each dune. Under such an assumption, the depth above or below the bottom of the dune will be assigned a positive or negative symbol, respectively, and only samples with a positive value of depth represent the desert landscape of concern in this paper. The OSL ages of sand samples were plotted against their depths in Fig. 6. As illustrated in Fig. 6, sand accumulation had already occurred as early as the beginning of the Holocene, around 11 ka; however, the present desert landscape characterized by dune accumulation began to develop rapidly during the latest 2 ka, especially within the latest 0.1 ka in this area.

5   Discussion

The dating results of sands beneath the bottom of the sand dunes around the JSL support the assertion that the initiation of sand accumulation can be traced back to the early Holocene, around 11 ka, and that sand accumulation

was replaced by clayey silty sand or sandy clay formed in a lake or swamp sometime before 6.7 ka. However, the sand accumulation sometime before 6.7 ka formed only the base of the present visual desert landscape characterized by sand dunes/hills. Moreover, until 2 ka, and particularly during the latest 0.1 ka, the sands began to accumulate rapidly at a large scale resulting in the formation of sand dunes and hills in a large area surrounding the JSL, as seen in the present desert landscape as shown in Fig. 6. Evidence from sand dunes in the southeast corner of the JSL, e.g., profiles WP414 and WP414-2, supports the assertion that the initiation of aeolian sand accumulation surrounding the JSL can be traced back to the early Holocene, around 11 ka. However, the sand accumulation initiated since ~11 ka was replaced by 5-cm-thick brownish red, consolidated fine sand, with calcium carbonate cementation (e.g., profile WP414) sometime before 6.4 ka (Fig. 3), supporting the existence of a short-time underwater environment sometime before 6.4 ka. Similarly, the sedimentary sequence in profile BS2 and BS4 supports the idea that a lake or swamp existed before 6.7 ka in the southeast corner of the JSL. Therefore, evidence of sedimentary sequence with ages from the southeast corner of the JSL supports the assertion

Table 3 OSL dating results related to the desert landscape surrounding the JSL

Profile	Sample	U/ppm	Th/ppm	K/%	D_e/Gy	Qualified/Total aliquots*	Grain size/μm	Water content /(wt %)	Depth /m	Cosmic ray dose rate /(Gy·ka⁻¹)	Total dose rate /(Gy·ka⁻¹)	Age/ka
WP414	OSL-2	0.95±0.06	3.01±0.13	1.70±0.11	14.83±1.20	6/15	90–125	5±5	0.37	0.24	2.31±0.17	6.42±0.71 ka
	WP414-100	0.81±0.05	2.32±0.1	1.86±0.06	25.77±2.08	15/24	90–125	15±5	1.0	0.21	2.26±0.11	10.93±1.04 ka
WP414-2	WP414-2-140	1.15±0.06	3.52±0.14	1.74±0.06	22.63±1.45	6/10	90–125	5±5	1.4	0.20	2.50±0.14	9.05±0.76 ka
BS2	OSL-4	1.37±0.07	3.13±0.13	1.55±0.11	15.32±1.01	7/12	90–125	5±5	0.74	0.25	2.28±0.17	6.73±0.76 ka
BS4	OSL-10	0.97±0.06	2.33±0.11	1.75±0.10	15.39±0.57	7/13	90–125	5±5	0.7	0.22	2.30±0.17	6.71±0.55 ka
S7	OSL-15	1.72±0.07	3.54±0.14	1.96±0.12	16.17±0.58	11/12	90–125	5±5	0.4	0.24	2.78±0.20	5.82±0.47 ka
B0719	B0719-60	1.20±0.06	3.00±0.12	1.54±0.05	0	7/12	90–125	5±5	0.6	0.23	2.60±0.14	<0.1 ka
	B0719-240	0.82±0.05	2.15±0.11	1.72±0.06	13.91±0.85	10/12	90–125	5±5	2.4	0.18	2.27±0.12	7.74±0.86 ka
JLT20130610	JLT20130610-140	1.20±0.06	4.63±0.17	2.00±0.06	2.21±0.14	8/12	90–125	5±5	1.4	0.20	2.83±0.15	0.78±0.06 ka
S64	S64-75	1.70±0.08	6.40±0.21	1.85±0.06	0	0/12	90–125	5±5	0.75	0.23	2.98±0.16	<0.1 ka
DS1	DS1-40	1.07±0.06	4.20±0.16	2.32±0.07	0	0/12	90–125	5±5	0.4	0.25	3.15±0.17	<0.1 ka
DS2	DS2-120	1.33±0.06	5.48±0.20	2.29±0.07	0	0/12	90–125	5±5	1.2	0.23	3.22±0.18	<0.1 ka
DS3	DS3-110	0.74±0.05	2.52±0.11	1.85±0.06	0	0/12	90–125	5±5	1.1	0.23	2.48±0.13	<0.1 ka
DS6	DS6-90	1.17±0.06	3.81±0.15	1.92±0.06	0.90±0.06	9/22	90–125	5±5	0.9	0.22	2.72±0.15	0.33±0.02ka
DS7	DS7-90	0.81±0.05	2.80±0.21	1.89±0.06	0	0/12	90–125	5±5	0.9	0.22	2.54±0.13	<0.1 ka

* The number of qualified aliquots represents the number of aliquots which are considered of either well-bleached or suitable for construction of a growth curve, and the total aliquots represent the number of aliquots that satisfied the three criteria mentioned in the text. For example, the numbers 15/24 in this volume means there are 24 aliquots satisfied the three criteria mentioned in the text and only 15 aliquots are considered well-bleached and suitable for being involved in the statistics and calculation of the D_e value for the sample WP414-100.
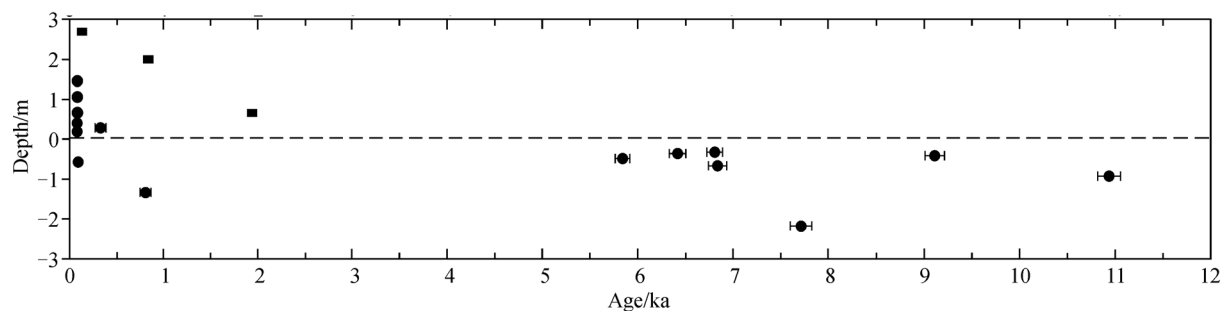
Fig. 6 Plot of OSL ages against the depth deviated from the assumed 0 depth line at the bottom of sand dunes/hills. The filled circles represent data of this study, and filled squares represent data referred from Fan et al. (2010).

that the sand accumulation was replaced by an ephemeral lake or swamp sometime before 6.7 ka. This assertion is also supported by the recognition of Zhao et al. (2012) obtained from the eastern neighboring Ulan Buh Desert that a unified Ulan Buh Paleolake, covering the present day JSL and the northern Ulan Buh Desert during 7.8–7.1 ka, broke apart after 6.5 ka. Sand accumulation has been reinitiated at many sites, e.g., BS2 BS4, S7, and WP414, since 6.4 ka. However, the sand accumulation before 2 ka did not form a well-preserved visual landscape. It was only during the latest 2 ka, and especially within the latest 0.1 ka, that sand accumulation rapidly developed to form the present desert landscape, which is characterized by visual sand dunes and hills.

The sand accumulation surrounding the JSL occurred during the Early Holocene, yet only in a limited area; however, the development of desert landscape was increased, especially during the latest 0.1 ka. This small area of sand accumulation took place in the southeast corner, close to the current location of the salt lake, as evidenced from profiles WP414, WP414-2, and B0719 (Fig. 1). Around 6.4 ka, sand accumulation expanded to the southwest corner of the current salt lake, as is supported by the sedimentary sequence in profile S7 (Fig. 1). During the latest 2 ka, the sand accumulation expanded to the point where it covered the entire area of the JSL, as is supported by sedimentary sequence from profiles WLD07A, JLT20130610, B0719, DS6, DS7, DS1, DS2, DS3, and S64 (Figs. 1 and 3). For example, sand accumulation began to occur southwest of the current location of the salt lake around 0.8 ka, as evidenced from site JLT20130610, and then expanded to the west, close to site DS6, around 0.3 ka. During the latest 0.1 ka, sand accumulation expanded from the current east and northeast banks of the JSL (e.g., sites B0719 and WLD07D) to the paleo-lakeshores with high altitudes ranging between 1,050 m and 1,080 m (e.g., sites DS1, DS2, DS3, DS7, and S64, see details in Fig. 1). Sand accumulation during the early Holocene (11- > 6.7 ka, likely before 7.8 ka as discussed above) is not an individual phenomenon in this area. This idea is supported by sand dune activity from the adjacent areas, which are similarly situated in the western frontier of the present East Asian

summer monsoon domain, such as the Ulan Buh Desert (Fan et al., 2010; Chen et al., 2014), the Hobq Desert (Sun et al., 2006; Li et al., 2007; Fan et al., 2013), the Otindag Sand Field (Lu et al., 2005; Zhou et al., 2005), and the Qaidam Basin, as well as in the deserts much closer to the present East Asian summer monsoon domain, such as the Mu Us Desert (Lu et al., 2005; Zhou et al., 2005) and Horqin Sand Land (Yang et al., 2010a). Widespread sand mobility was recorded most extensively at many sites along the desert margin in northern China between 11.5 and 8 ka, which was interpreted by low effective moisture at the desert's margin, possibly resulting from a dynamic link between a strong monsoon circulation and enhanced subsidence in dry lands north of the monsoon core, together with greater-than-modern evapotranspiration (Mason et al., 2009). However, such an interpretation conflicts with the idea of Yang et al. (2004, 2010b) with evidence of high lake levels and wetter climate beginning at ca. 10 ka and lasting until the mid-Holocene in the Badain Jaran Desert. Meanwhile, a transition from a shallow water lake to a deep water lake occurred since around 8 ka in Lake Bosten, which is situated in Xinjiang, the westerly dominant area (Fan et al., 2007). This transition might reflect a background of strong westerlies versus weak East Asian summer monsoon thereafter (Chen et al., 2006). To date, we do not possess any evidence of intensified human activity during the early Holocene in the area of Jilantai, as studied in this paper. Therefore, together with sand dune mobility in the western frontier belt of the present East Asian summer Monsoon domain, we consider that the early Holocene sand accumulation around the JSL likely reflects an environmental character of relatively low effective moisture around Jilantai, occurring for as yet unknown reasons.

No obvious sand dune mobility was observed during 8-3 ka in the Mu Us and Horqin deserts, which are situated within the present East Asian summer monsoon domain (Lu et al., 2005; Zhou et al., 2005, 2009; Mason et al., 2009; He et al., 2010; Yang et al., 2012). In addition, all of the Chinese sand fields were almost completely covered by vegetation during the 9–5 ka (Lu et al., 2013). This evidence supports a humid climatic condition with strong

monsoon precipitation. However, succeeding the recession or shrinkage of the unified Ulan Buh paleolake after 6.5 ka (Zhao et al., 2012), sand accumulation occurring since 6.4 ka is supported by sedimentary sequence at sites BS4 and WP414, as well as the sand dune on the spring mound S7. The sand accumulation during this interval was synchronous with both the sand accumulation in the eastern neighboring Ulan Buh Desert (Fan et al., 2010) and Hobq Desert (Sun et al., 2006; Li et al., 2007; Fan et al., 2013), as well as the drought event revealed by the sedimentary sequence in the lakes in the Tengger Desert, approximately 100 km south of the JSL (Chen et al., 2003; Long et al., 2007). This type of dry event was also documented by the interruption of Holocene soil in the Guanzhong Basin in the present East Asian summer monsoon domain (Chen et al., 2007). Therefore, together with other documents on this marginal belt and in the Guanzhong Basin, the sand accumulation around JSL from approximately 6.4 to 5.8 ka likely supports a dry interval of weak summer monsoon within the Holocene Optimum.

Rapid sand accumulation around the JSL started around 2 ka and expanded during the period of 0.8 ka and 0.3 ka; however, it was only during the latest 0.1 ka that the present desert landscape formed, being primarily composed of sand dunes over a large area. The rapid development of sand dunes around 0.8 ka is difficult to elucidate from climatic conditions due to the strength of the East Asian summer monsoon during that time, which is supported by geological documents for the present East Asian summer monsoon domain, e.g., the loess/soil sequence in the Guanzhong Basin (Zhao et al., 2007) and stalagmite records from the Wanxiang Cave and the Hulu Cave (Wang et al., 2005; Zhang et al., 2008). However, wars with Mongolia ensued in Jilantai and in the large surrounding areas around 0.8 ka (1211 A.D.) (Tan, 1991). Therefore, it is logical to deduce that rapid sand accumulation during that time was a result of intensified human activity.

At about 0.3 ka, the expanse of sand accumulation not only took place in the area surrounding the JSL, but also in the areas on the western margin of the present East Asian summer monsoon domain, to its east, e.g., the Mu Us Desert and Otingdag Desert (Zhou et al., 2009), in addition to the southern margin of the Horqin (Yang et al., 2010a; Lu et al., 2013) and the Hulun Buir (Lu et al., 2013). This large scale sand accumulation along the western frontier of the present East Asian summer monsoon was likely a result of relatively low effective moisture conditions. This strengthening of sand accumulation was synchronous with the Little Ice Age at the end of the 17th century, characterized by dry and cold conditions in western China (Qin, 2005). At that time, the East Asian summer monsoon was weak, which was supported by the oxygen isotope curve of stalagmite documents from the Wanxiang Cave (Zhang et al., 2008). Moreover, large scale salt mining in the JSL began in 1736 A.D. (Yu et al., 2001); therefore, the

rapid sand accumulation that occurred around 0.3 ka is considered to be the result of intensified human activities under the dry and cold climate conditions of that time.

The large scale development of the present desert landscape covering the entire area of the JSL occurred within the last 0.1 ka. During this time, the East Asian summer monsoon was strong, as revealed from the oxygen isotopic curves of stalagmite in the Wanxiang Cave (Zhang et al., 2008). However, it was prevailed by the drier and warmer climatic condition of arid central-eastern Asia during the latest 100 years (Wang, 2006), which was demonstrated by decreased precipitation and increased evaporation since 1964 A.D. (Yu et al., 2001). On the other hand, a large area of natural vegetation in the Alashan Plateau was extensively destroyed through cultivation (Liu and Gao, 2007), as a result of huge immigration and changes from animal herding to cultivation since the early 1950s. The natural environment seriously deteriorated in the vast area around the Jilantai (Liu and Gao, 2007), especially after the accelerated development of salt mining in the JSL due to the development of mechanization in 1975 (Yu et al., 2001). For example, 67,000 ha of Haloxylon ammodendron surrounding the JSL during the 1960s became extinct in the early 1980s (Geng and Chen, 1990; Gao, 1996; Liu and Zhang, 2000; Yu et al., 2001). In brief, the rapid development of the present desert landscape in large areas surrounding the JSL accelerated by intensified industrial activities and cultivation under a dry and warm climatic condition during the latest 0.1 ka.

6   Conclusions

It is clear from the sedimentary sequence of the current visual sand dunes and hills surrounding the JSL as studied in this paper, that the sand desert landscape developed above either lacustrine and bog deposits, or paleo-lakeshores of lakes in the Jilantai Basin. Dating results support that sand accumulation around the JSL can be traced back to the early Holocene, as early as 11 ka; however, rapid development of the present desert landscape occurred within the latest 0.1 ka. Comparison with climatic documents and historical records in the neighboring areas supports the assertion that sand accumulation surrounding the JSL before 2 ka (11−7.8 ka and 6.4−5.8 ka intervals) likely reflects an environmental character of relatively low effective moisture around the Jilantai, occurring for, as yet, unknown reasons. Moreover, the rapid development of the sand desert landscape over large areas of the Jilantai was accelerated by intensified human activities under a dry and warm climatic condition within the latest 0.1 ka.

References

Aitken M J (1985). Thermoluminescence Dating. London: Academic Press, 61–112

An Z S, Huang Y S, Liu W G, Guo Z T, Steven C, Li L, Warren P, Ning Y F, Cai Y J, Zhou W J, Lin B H, Zhang Q L, Cao Y N, Qiang X K, Chang H, Wu Z K (2005). Multiple expansions of C4 plant biomass in East Asia since 7 Ma coupled with strengthened monsoon circulation. Geology, 33(9): 705–708

Banerjee D, Murray A S, Bøtter-Jensen L, Lang A (2001). Equivalent dose estimation using a single aliquot of polymineral fine grains. Radiat Meas, 33(1): 73–94

Chen F H, Cheng B, Zhao H, Fan Y X, Madsen D B, Jin M (2007). Post-glacial climate variability and drought events in the monsoon transition zone of western China. In: Madsen et al., eds. Late Quaternary Climate Change and Human adaptation in arid China, 25–40

Chen F H, Fan Y X, Chun X, Madsen D B, Oviatt C G, Zhao H, Yang L P, Sun Y (2008). Preliminary Research on Megalake Jilantai-Hetao in the arid areas of China during the Late Quaternary. Chin Sci Bull, 53 (11): 1725–1739

Chen F H, Huang X Z, Yang M L, Yang X L, Fan Y X, Zhao H (2006). Westerly dominated Holocene climate model in arid central Asia—-Case study on Bosten Lake, Xinjiang, China. Quaternary Sciences, 26(6): 881–887 (in Chinese)

Chen F H, Li G Q, Zhao H, Jin M, Chen X M, Fan Y X, Liu X K, Wu D, Madsen D (2014). Landscape evolution of the Ulan Buh Desert in northern China during the late Quaternary. Quat Res, 81(3): 476–487

Chen F H, Wu W, Zhu Y, Holmes J A, Madsen D B, Jin M, Oviatt C G (2003). A Mid-Holocene drought interval as evidenced by lake desiccation in the Alashan Plateau, Inner Mongolia, China. Chin Sci Bull, 48(14): 1401–1410

Chun X, Chen F H, Fan Y X, Xia D S, Zhao H (2008). Formation of Ulan Buh Desert and its environmental changes during the Holocene. Front Earth Sci China, 2(3): 327–332

Fan Y X (2008). Study on the evolution of Jilantai-Hetao Megalake focusing on optical dating of lakeshore sediments. Dissertation for Ph.D degree. Lanzhou: Lanzhou University, 1–159 (in Chinese)

Fan Y X, Chen F H, Fan T L, Zhao H, Yang L P (2010). Sedimentary documents and Optically Stimulated Luminescence (OSL) dating for formation of the present landform of the northern Ulan Buh Desert, northern China. Science China Earth Sci, 53(11): 1675–1682

Fan Y X, Chen X L, Fan T L, Jing M, Liu J B, Chen F H (2013). Sedimentary and OSL dating evidence for the development of the present Hobq Desert landscape, northern China. Science China Earth Sci, 56(12): 2037–2044

Fan Y X, Zhao H, Chen F H, Huang X Z, Yang M L (2007). OSL dating of lacustrine sediments from Lake Bosten. Quaternary Sciences, 27 (4): 568–575 (in Chinese)

Gao Y (1996). The environmental evolution and sand injury cause in Jilantai Salt Lake. Arid Zone Research, 13(4): 54–57 (in Chinese)

Geng K, Chen Y F (1990). Formation, development and evolution of Jilantai Salt Lake, Inner Mongolia. Acta Geogr Sin, 45(3): 341–349 (in Chinese)

Geng K, Hu C Y (1989). The evolution trend of the Salt-lake in Jilantai area, Inner Mongolia. Journal of Beijing Normal University Science, 3: 86–91 (in Chinese)

Geng K, Hu C Y (1990). Environmental degradation and comprehensive treatment approach of Jilantai Salt Lake. Areal Research and Development, 9(6): 49–52 (in Chinese)

He Z, Zhou J, Lai Z P, Yang L H, Liang J M, Long H, Ou X J (2010). Quartz OSL dating of sand dunes of Late Pleistocene in the Mu Us Desert in northern China. Quat Geochronol, 5(2–3): 102–106

Li S H, Chen Y Y, Li B, Sun J M, Yang L R (2007). OSL dating of sediments from deserts in northern China. Quat Geochronol, 2(1–4): 23–28

Liu K L, Gao B Z (2007). Ecological environment deterioration and social culture changes of Alxa. Beijing: Academy Press, 111–120 (in Chinese)

Liu X Q, Zhang H (2000). Studies on remote sensing monitoring of desertification and its defence and control of Jilantai Salt Lake. Journal of Salt Lake Research, 8(2): 1–5 (in Chinese with English Abstract)

Long H, Wang N A, Li Y, Ma H Z, Zhao Q, Chen H Y, Ma Y Z (2007). Mid-Holocene climate variations from lake records of the East Asian Monsoon margin: a multi-proxy and geomorphological study. Quaternary Sciences, 27(3): 372–381 (in Chinese with English Abstract)

Lu H Y, Miao X D, Zhou Y L, Mason J, Zhang J F, Zhou L P, Yi S W (2005). Late Quaternary aeolian activity in the Mu Us and Otindag dunefields (north China) and lagged response to insolation forcing. Geophys Res Lett, 32(21): L21716

Lu H Y, Yi S W, Zhou Y L, Xu Z W,, Zhu F Y, Zeng L, Zhu F Y, Feng H, Dong L N, Zhuo H X, Yu K F, Mason J, Wang X Y, Chen Y Y, Lu Q, Wu B, Dong Z B, Qu J J, Wan X M, Guo Z T (2013). Chinese deserts and sand fields in Last Glacial Maximum and Holocene Optimum. Chin Sci Bull, 58(23): 2775–2783

Mason J, Lu H Y, Zhou Y L, Miao X D, Swinehart J B, Liu Z, Goble R J, Yi S (2009). Dune mobility and aridity at the desert margin of northern China at a time of peak monsoon strength. Geology, 37(10): 947–950

Murray A S, Wintle A G (2000). Luminescence dating of quartz using an improved single aliquot regenerative-dose protocol. Radiat Meas, 32 (1): 57–73

Pang X L, Hu D S (2009). Environment evolution and salt forming process of Jilantai Salt Lake since 22 ka BP. J Desert Res, 29(2): 193–199 (in Chinese)

Prescott J R, Hutton J T (1994). Cosmic ray contributions to dose rates for luminescence and ESR dating: large depths and long-term variations. Radiat Meas, 23(2–3): 497–500

Qin D H (2005). Climate change and environment change and their projection. Beijing: Science Press, 78–79 (in Chinese)

Roberts H (2012). Testing Post-IR IRSL protocols for minimizing fading in feldspars, using Alaskan loess with independent chronological control. Radiat Meas, 47(9): 716–724

Sun J M, Li S H, Han P, Chen Y Y (2006). Holocene environmental changes in the central Inner Mongolia, based on single-aliquot quartz Optical dating and multi-proxy study of dune sands. Palaeogeogr Palaeoclimatol Palaeoecol, 233(1–2): 51–62

Tan Q X (1991). Concise Historical Atlas of China. Beijing: Sino Maps Press, 51–52 (in Chinese)

Wang F Y (2001). Satellitic radar remote sensing studies on evolution of Jilantai Salt Lake. Remote Sensing for Land & Resources, 4: 35–39 (in Chinese)

Wang J S (2006). Study on regional climate response to global warming in the Arid Central-East Asia over the past 100 years. Dissertation for Ph.D degree. Lanzhou: Lanzhou University, 31–81 (in Chinese)

Wang S M, Dou K S (1998). Chinese Lakes. Beijing: Science Press, 327–328 (in Chinese)

Wang T (1989). Comparative study on desertification of the typical areas in Northern China. J Desert Res, 9(1): 113–136 (in Chinese)

Wang Y J, Cheng H, Edwards R L, He Y Q, Kong X G, An Z S, Wu J Y, Kelly M I, Dykoski C A, Li X D (2005). The Holocene Asian Monsoon: links to solar changes and north Atlantic climate. Science, 308(5723): 854–857

Wintle A G, Murray A S (2006). A review of quartz optically stimulated luminescence characteristics and their relevance in single-aliquot regeneration dating protocols. Radiat Meas, 41(4): 369–391

Yang L H, Wang T, Zhou J, Lai Z P, Long H (2012). OSL chronology and possible forcing mechanisms of dune evolution in the Horqin dunefield in northern China since the Last Glacial Maximum. Quat Res, 78(2): 185–196

Yang L H, Zhou J, Lai Z P, Long H, Zhang J R (2010a). Late glacial and Holocene dune evolution in the Horqin dunefield of the northern China based on luminescence dating. Palaeogeogr Palaeoclimatol Palaeoecol, 296(1–2): 44–51

Yang L P, Chen F H, Chun X, Fan Y X, Sun Y, Madsen D B, Zhang X (2008). The Jilantai Salt Lake shorelines in Northwestern arid China revealed by remote sensing images. J Arid Environ, 72(5): 861–866

Yang X P, Ma N, Dong J F, Zhu B Q, Xu B, Ma Z B, Liu J Q (2010b). Recharge to the inter-dune lakes and Holocene climatic changes in the Badain Jaran Desert, western China. Quat Res, 73(1): 10–19

Yang X P, Rost K T, Lehmkuhl F, Zhu Z D, Dodson J (2004). The evolution of dry lands in northern China and in the republic of Mongolia since the Last Glacial Maximum. Quat Int, 118–119: 69–85

Yu S S, Bai F Y, Li H J (2001). Resource Environment and Sustainable Development Research of Jilantai Salt Lake. Beijing: Science Press, 129–140 (in Chinese)

Zhang P Z, Cheng H, Edwards R L, Chen F H, Wang Y J, Yang X L, Liu J, Tan M, Wang X F, Liu J H, An C L, Dai Z B, Zhou J, Zhang D Z, Jia J H, Jin L Y, Johnson K R (2008). A test of climate, sun, and cultural relationships from an 1810-year Chinese cave records. Science, 322(5903): 940–942

Zhao H, Chen F H, Li S H, Wintle A G, Fan Y X, Xia D S (2007). A record of Holocene climate change in the Guanzhong Basin, China, based on optical dating of a loess-palaeosol sequence. Holocene, 17(7): 1015–1022

Zhao H, Li G Q, Sheng Y W, Jin M, Chen F H (2012). Early-middle Holocene lake-desert evolution in northern Ulan Buh Desert, China. Palaeogeogr Palaeoclimatol Palaeoecol, 331–332: 31–38

Zhou Y L, Lu H Y, Zhang J F, Mason J A, Zhou L P (2009). Luminescence dating of sand-loess sequences and response of Mu Us and Otindag Sandfields (North China) to climatic changes. J Quaternary Sci, 24(4): 336–344

Zhou Y L, Lu H Y, Zhang J F, Zhou L P, Miao X D, Mason J A (2005). Active and inactive phases of sand dune in Mu Us and Otindag Sandlands during Late Quaternary suggested by OSL dating. J Desert Res, 25(3): 342–350 (in Chinese)